SUPPLEMENTARY FIGURES

Suppl. Figure 1: Identification and comparative expression levels of ARH3 and PARG transcripts in various cells. (a) A 353-bp fragment of the ARH3 mRNA was detected by RT-PCR analysis with cDNA from HeLaS3 cells (lane 1), 293 cells (lane 2), HepG2 cells (lane 3) and SH-SY5Y cells (lane 4). Lane 5: H_2O control. (b) Specific fragments of alternatively spliced mRNAs encoding PARG55 (black arrows; 203 bp in lanes 1-3, 234 bp in lanes 5-7) and PARG60 (white arrows; 280 bp lanes 1-3, 311 bp lanes 5-7) were co-amplified from cDNA preparations from 293 cells (lanes 1 and 5), HepG2 cells (lanes 2 and 6) and SH-SY5Y cells (lanes 3 and 7). Lanes 4 and 8: H_2O control. (c) Specific fragments of alternatively spliced mRNAs encoding PARG55 (black arrows; 203 bp in lane 1, 234 bp in lane 2) and PARG60 (white arrows; 280 bp in lane 1, 311 bp in lane 2) were co-amplified from cDNA preparations from human PBMCs. Asterisks in (b) and (c) indicate fragments that were confirmed by DNA sequence analyses. Bands crossed out (x) in lane 1 of (c) were PCR products composed of sequences unrelated to the human PARG gene. For primer combinations see Experimental Procedures. DNA fragments were separated on 2.5% agarose gels. The sizes (bp) of selected marker bands are indicated. (d) Expression levels of the transcripts encoding ARH3 (white bars) and the sum of PARG55 and PARG60 mRNA (hatched bars) were determined by qRT-PCR on cDNA preparations from 293, HepG2, HeLaS3 and SH-SY5Y cell lines and compared to the mRNA levels of total PARG transcripts (grey + hatched bars). Human PARG55 and PARG60 mRNA accounted for only a minor fraction of total PARG transcripts. Human ARH3 transcript levels exceeded the levels of total PARG mRNAs. Data are from three experiments each performed in triplicate.

Suppl. Figure 2: Human PARG55 and PARG60 display different cellular distributions. Human PARG55, PARG55(ex5) and PARG60 were expressed as C-terminally FLAG-tagged proteins in HeLaS3 cells and detected by FLAG immunocytochemistry (FLAG). Human PARG55 and PARG55(ex5) co-localized with the green fluorescence of co-expressed EGFP targeted to mitochondria (mitoEGFP). Human PARG60 co-localized with the cytosolic portion of co-expressed untargeted EGFP (cytoEGFP) and not with mitochondrial EGFP.

Suppl. Figure 3: The expression level of mitoPARP1cd correlates with PAR content in mitochondria. MEFs from wild-type mice were transfected with mitoPARP1cd and subjected to PAR immunocytochemistry. The scatter plot shows the relationship of PAR and EGFP intensities (n = 33).

Suppl. Figure 4: Targeting small cytosolic PARG isoforms to the mitochondrial matrix. Human PARG55, PARG55(ex5) and PARG60 were endowed with an authentic N-terminal mitochondrial targeting sequence (MTS), expressed as C-terminally FLAG-tagged proteins in HeLaS3 cells and visualized by FLAG immunocytochemistry (FLAG). All MTS-PARG isoforms co-localized with co-expressed EGFP targeted to mitochondria. MTS-PARG60 did no longer co-localize with the cytosolic portion of co-expressed untargeted EGFP (cytoEGFP).

Suppl. Figure 5: (a) Quantification of fluorescence micrographs from immunocytochemistry analyses shown in Figs. 4 and 5. Co-expression of mitoPARP1cd and small human PARG isoforms within mitochondria resulted in a significant decrease in mitochondrial PAR content, when exon 5-encoded amino acids were present in the PARG primary structures [PARG55(ex5), MTS-PARG55(ex5) and MTS-PARG60(ex5)]. Quantification of EGFP fluorescence and FLAG signal intensities confirmed comparable expression levels. Data are from up to five experiments. Mean ± S.E.M., $P^{***} < 0.001$ (one-way *ANOVA* with *post hoc* Bonferroni test). (b) PAR, FLAG and EGFP immunoblot analyses of lysates from 293 cells expressing mitoPARP1 along with C-terminally FLAG-tagged PARG55 (lane 1), PARG55(ex5) (lane 2), MTS-PARG60(ex5) (lane 4) and MTS-PARG60 (lane 5). Lane 3 was loaded with lysate from cells expressing mitoPARP1cd in presence of the FLAG-vector. β-tubulin was used as loading control.

Presence of PARG isoforms containing exon 5-encoded amino acids decreased the mitochondrial PAR content even when expressed at far lower levels.

Suppl. Figure 6: Confirmation of the specificity of the RT-PCRs shown in Fig. 5. Nested RT-PCR analyses using the same primer combinations as in Fig. 5 were performed using cDNA preparations from 3T3 cells as template. The elongation step was prolonged from 30 sec to 3 min. PCR-products indicated by asterisks derived from transcripts specific for mPARG110 and mPARG101. The main PCR product from the primary PCR (crossed out (x) in lane 1), did not contain any DNA sequence of the mPARG gene.

Suppl. Figure 7: Immunoblot analysis of lysates from MEFs confirmed the absence of ARH3 protein in *ARH3*$^{-/-}$ mice.

Suppl. Figure 8: Absence of ARH3 protects matrix-accumulated PAR from degradation. PAR and EGFP immunoblot analyses of lysates from wild-type and *ARH3*$^{-/-}$ MEFs transiently expressing mitoPARP1cd. One day post transfection, cells were incubated in the absence or presence of 5 μM PJ-34 for indicated time periods. Data are representative of three experiments.

Suppl. Figure 9: Stable knockdown of PARG gene expression in *ARH3*$^{-/-}$ cells. *ARH3*$^{-/-}$ cells were stably transfected with a plasmid encoding shRNA specific for all known mature mPARG transcripts (shPARG). Control cells expressed an irrelevant shRNA (shControl) or were transfected with a plasmid harboring only the H1 RNA promoter (shEmpty). PARG gene expression was quantified by qRT-PCR analyses and normalized to GAPDH. The mean ± S.E.M. was obtained from four different samples. $P^* < 0.05$ (one-way *ANOVA* with *post hoc* Bonferroni test).

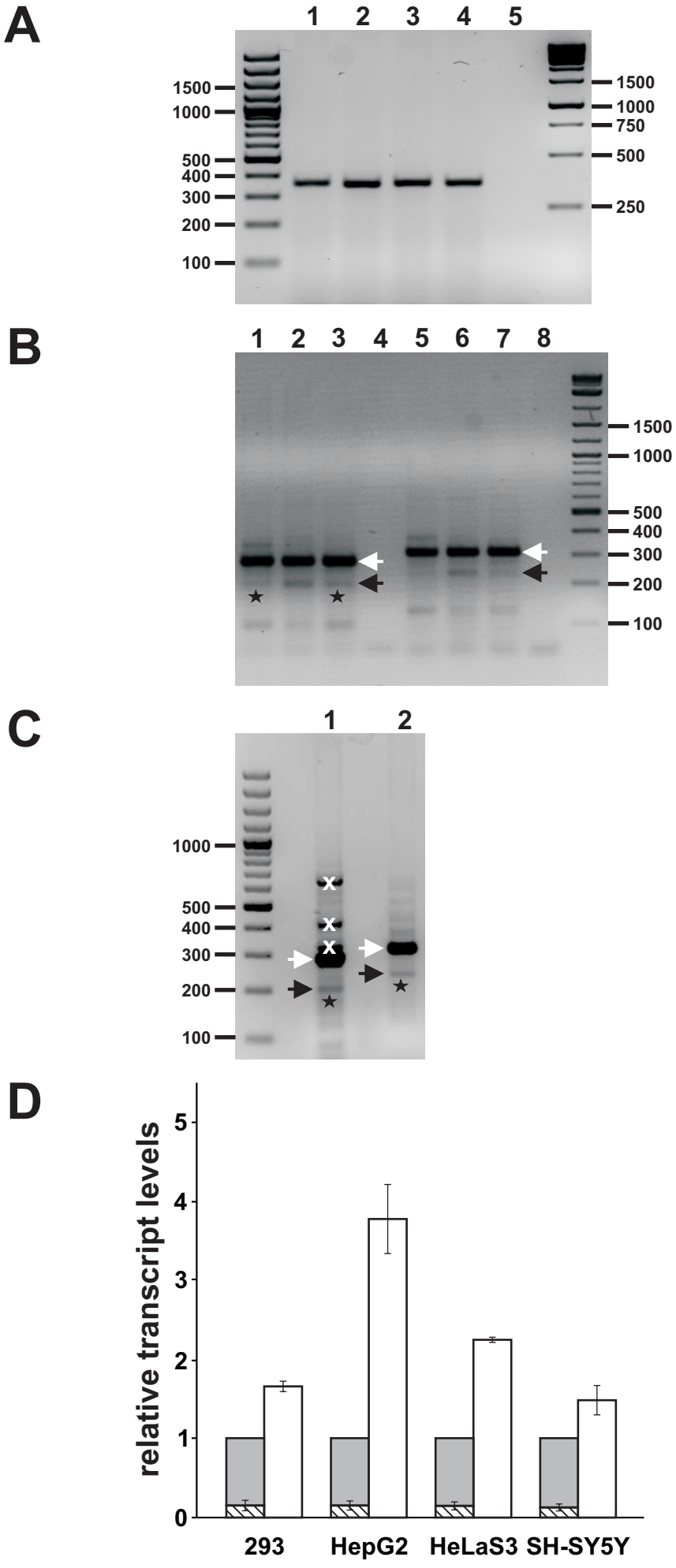

Supplementary Figure 1

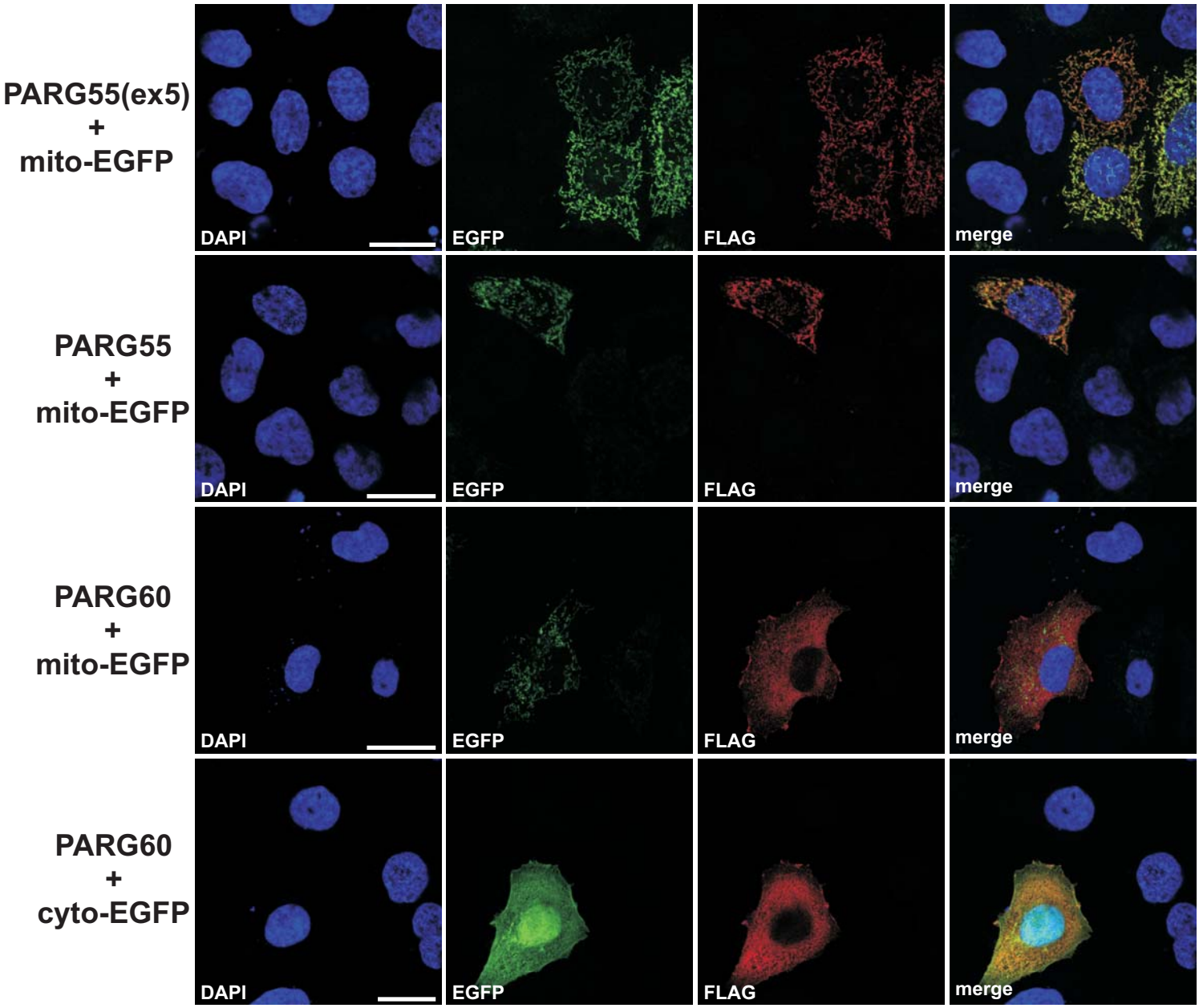

Supplementary Figure 2

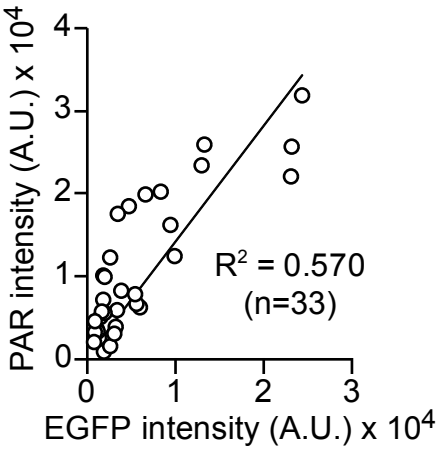

Supplementary Figure 3

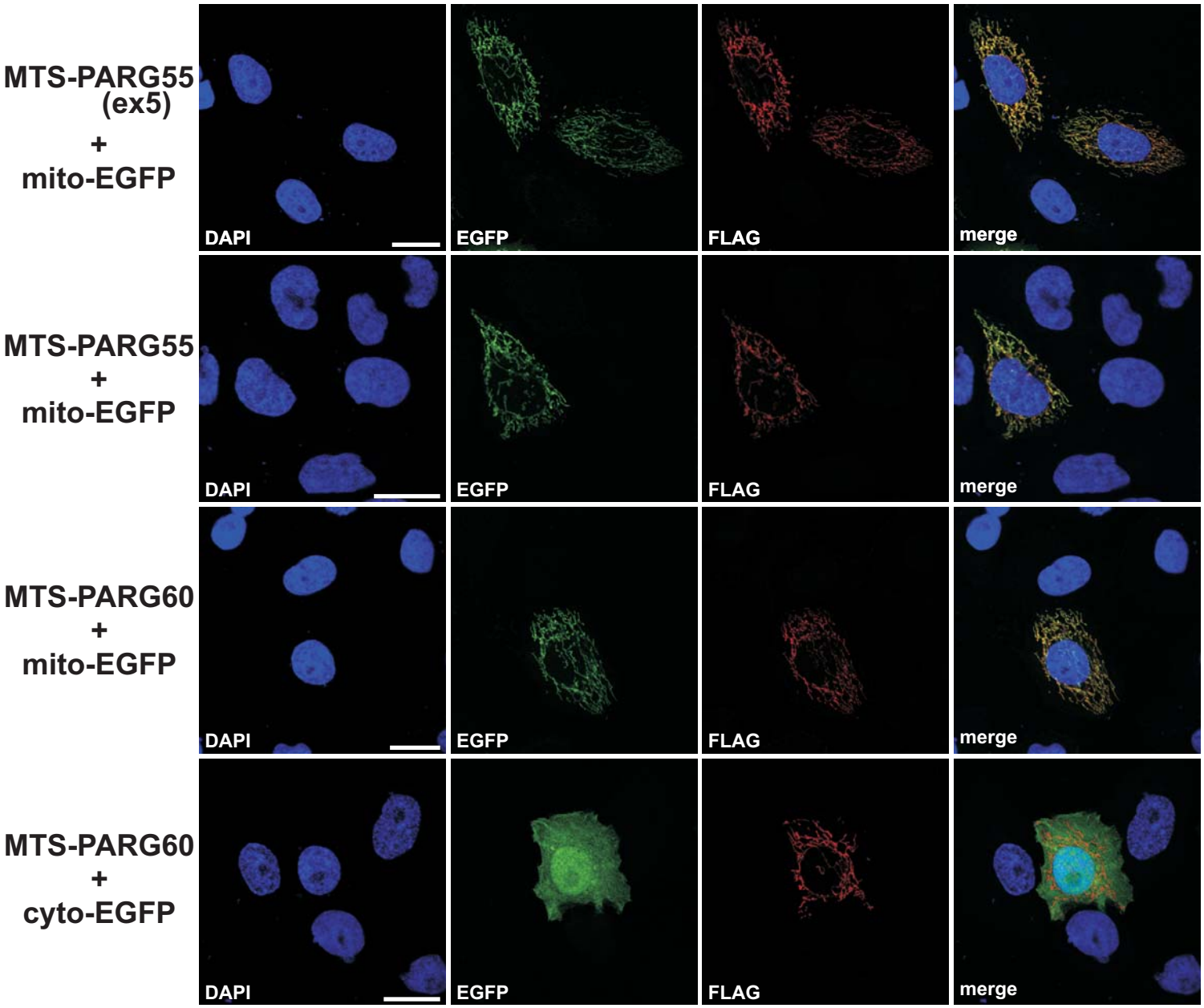

Supplementary Figure 4

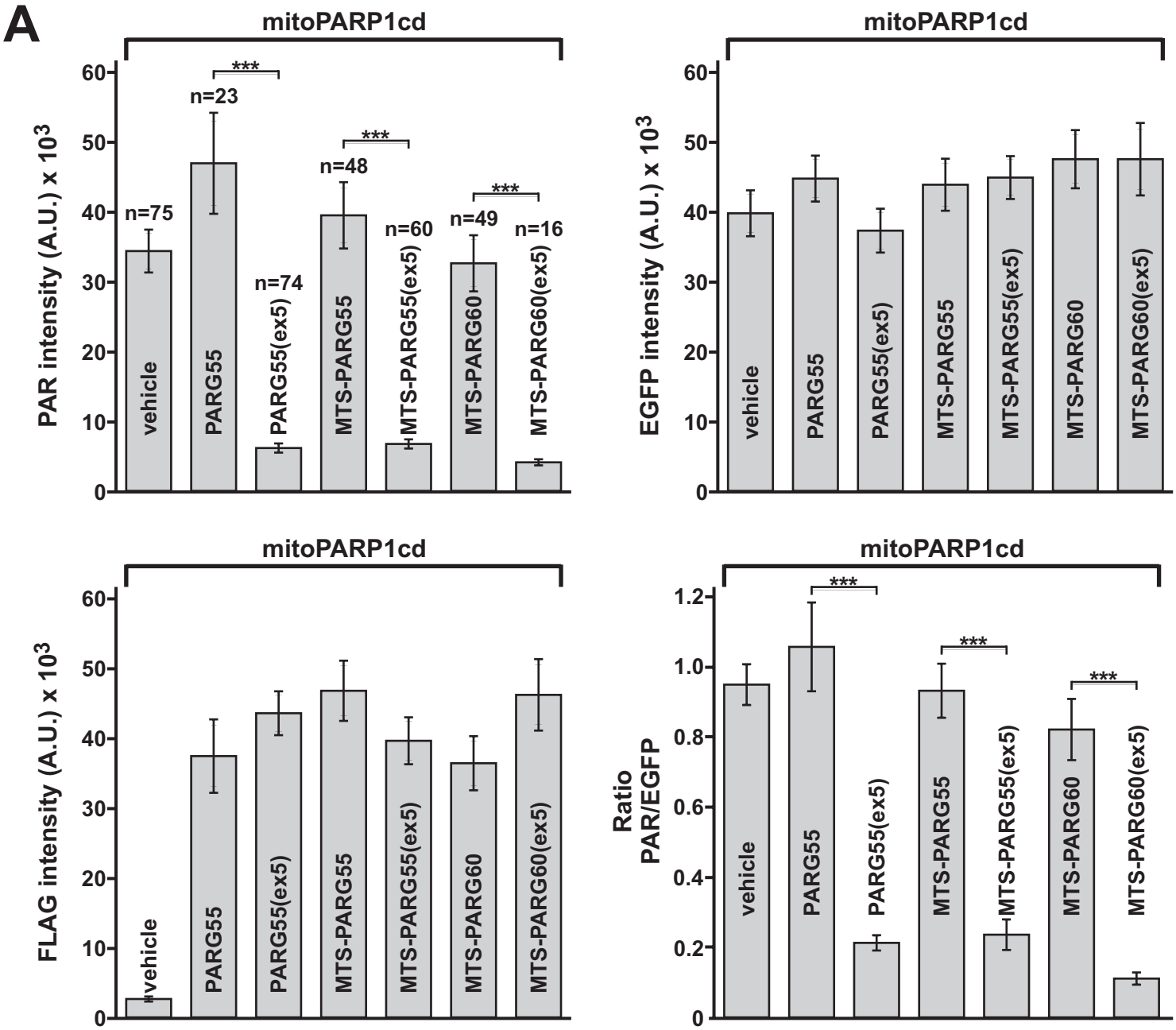

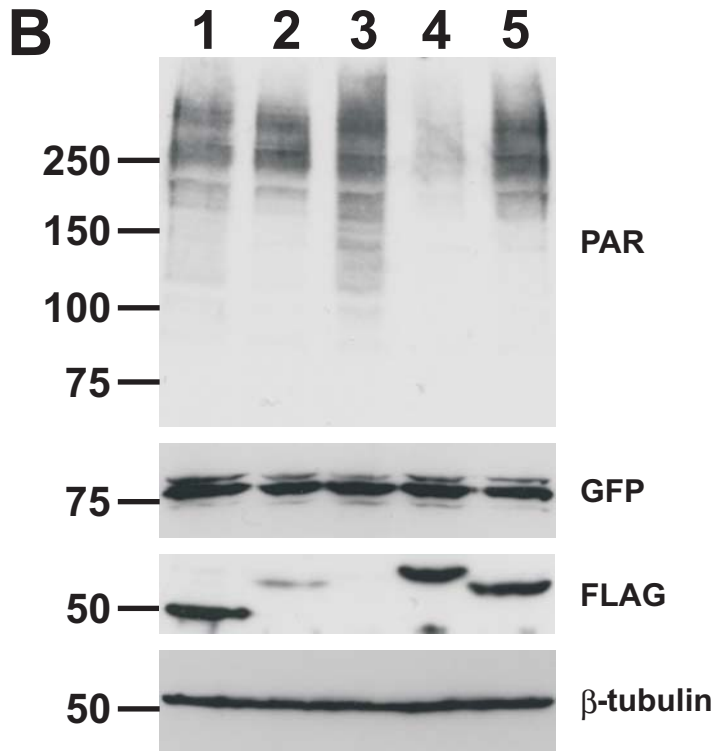

Supplementary Figure 5

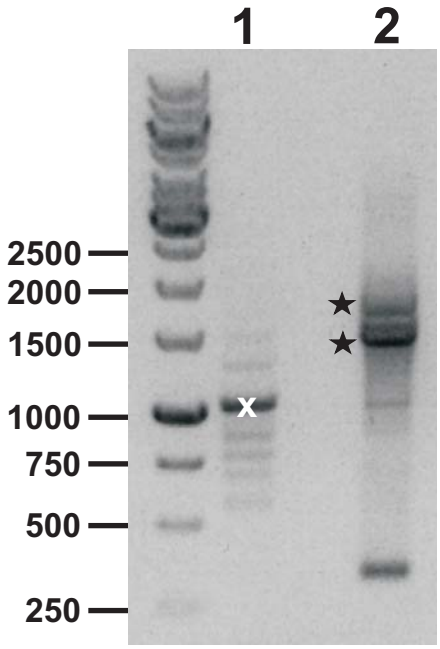

Supplementary Figure 6

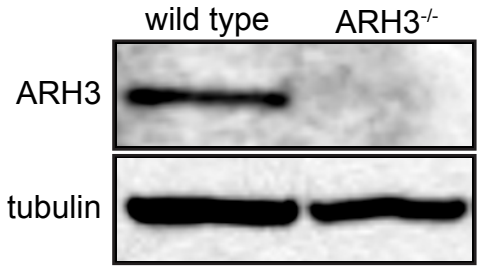

Supplementary Figure 7

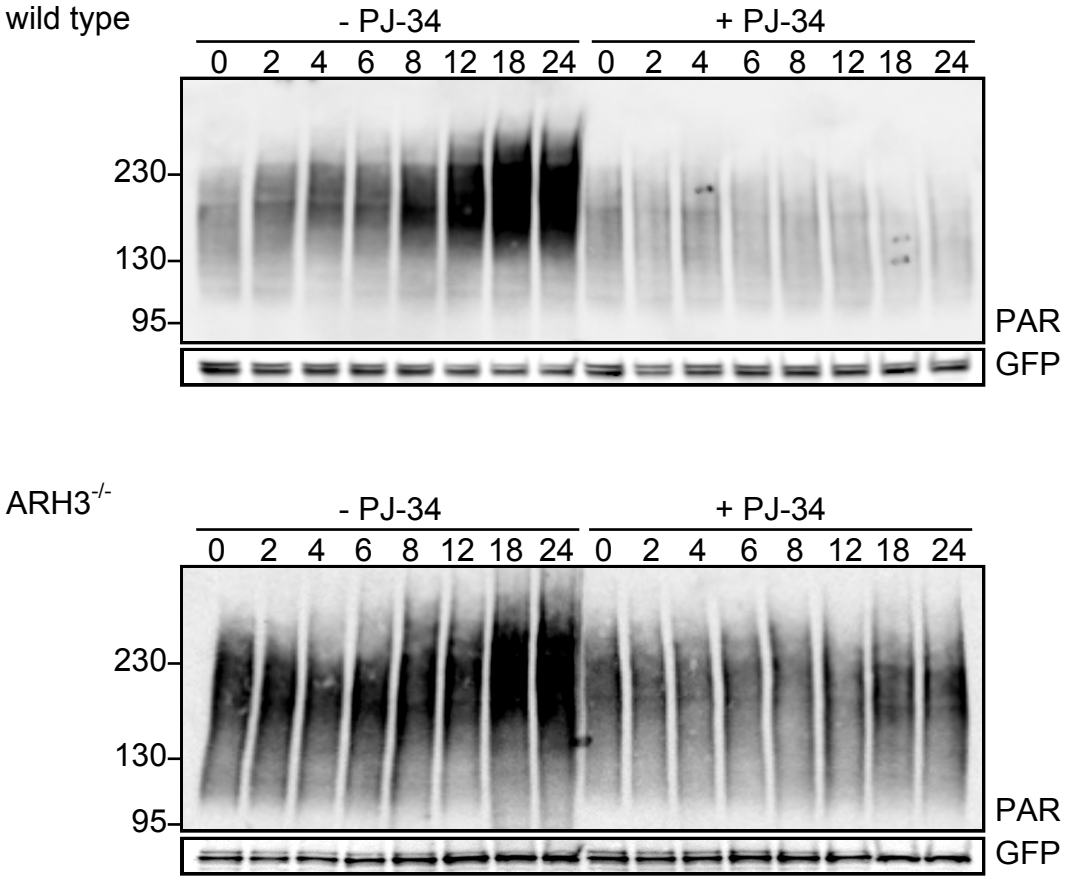

Supplementary Figure 8

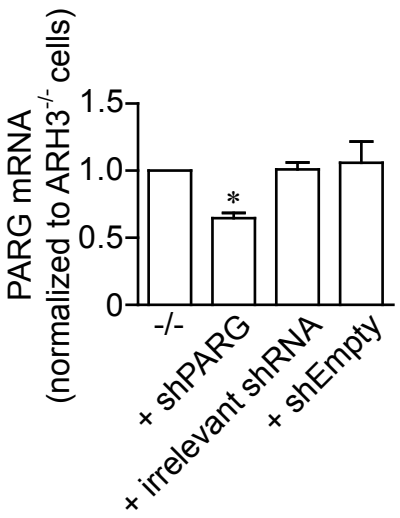

Supplementary Figure 9